Available online at www.sciencedirect.com
ScienceDirect
Journal of the European Ceramic Society 29 (2009) 2343–2353
www.elsevier.com/locate/jeurceramsoc

Photocatalytic activities of N-doped nano-titanias and titanium nitride

Zhice Zhang [a,b], Josephine B.M. Goodall [a], David J. Morgan [c], Sonal Brown [a], Robin J.H. Clark [a], Jonathan C. Knowles [d], Nicola J. Mordan [d], Julian R.G. Evans [a], Albert F. Carley [c], Michael Bowker [c], Jawwad A. Darr [a,*]

[a] *Christopher Ingold Laboratories, University College London, 20 Gordon Street, London, WC1H 0AJ, UK*
[b] *School of Engineering and Materials Science, Queen Mary, University of London, Mile End Road, London, E1 4NS, UK*
[c] *School of Chemistry, Cardiff University, Main Building, Park Place, Cardiff, CF10 3AT, UK*
[d] *Division of Biomaterials and Tissue Engineering, UCL Eastman Dental Institute, 256 Gray's Inn Road, London, WC1X 8LD, UK*

Received 5 November 2008; received in revised form 28 January 2009; accepted 12 February 2009
Available online 21 March 2009

Abstract

TiO_2 doped with various loadings of nitrogen was prepared by nitridation of a nano-TiO_2 powder in an ammonia/argon atmosphere at a range of temperatures from 400 to 1100 °C. The nano-TiO_2 starting powder was produced in a continuous hydrothermal flow synthesis (CHFS) process involving reaction between a flow of supercritical water and an aqueous solution of a titanium salt. The structures of the resulting nanocatalysts were investigated using powder X-ray diffraction (XRD) and Raman spectroscopy. Products ranging from N-doped anatase TiO_2 to phase-pure titanium nitride (TiN) were obtained depending on post-synthesis heat-treatment temperature. The results suggest that TiN started forming when the TiO_2 was heat-treated at 800 °C, and that pure phase TiN was obtained at 1000 °C after 5 h nitridation. The amounts and nature of the Ti, O and N at the surface were determined by X-ray photoelectron spectroscopy (XPS). A shift of the band-gap to lower energy and increasing absorption in the visible light region, were observed by increasing the heat-treatment temperature from 400 to 700 °C.

Keywords: TiO_2; Powders-gas phase reaction; Grain growth; Optical properties and continuous hydrothermal flow synthesis

1. Introduction

Titanium dioxide (TiO_2) is used in a wide range of applications including pigments for white paints,[1,2] dielectric resonators,[3] gas sensors,[4,5] and catalysts.[6] Apart from these, TiO_2 (particularly in the anatase form) is the most widely used photocatalyst. As TiO_2 is illuminated with light of wavelengths shorter than *ca*. 388 nm, absorption of a photon with sufficient energy leads to charge separation due to electron promotion to the conduction band and generation of holes in the valence band. These holes react with water molecules or hydroxide ions to produce hydroxyl radicals, which can oxidize organic species. The photocatalytic process has many applications, for example to water purification,[7,8] self-cleaning of windows,[9–11] air purification,[12–14] pollutant or organic molecule destruction,[15,16] and production of antibacterial coatings.[17–19] Since *ca*. 97% of the solar spectrum has wavelengths >388 nm,[20] much of it cannot readily be used by pure titania directly. Therefore, various dopants are often introduced into the titania lattice either to decrease the band-gap or to introduce intra-band-gap states, which allow activation by visible light.[21,22]

Recently, photocatalysts based upon titanium dioxide activated by visible light have been obtained by doping nitrogen,[13,22–24] sulfur,[25] or fluorine[26] into the host lattice. These anionic dopant species were found to be more effective than transition-metal dopants, with respect to stability of the catalyst.[27] The red shift of the band-gap into the visible range, makes it possible to carry out a wide range of photocatalytic investigations under visible light (wavelength range 380–750 nm). Asahi et al.[23] first reported that band-gap narrowing by N-doping in TiO_2 yields material with high photocatalytic activities on irradiation with visible light. They prepared N-doped TiO_2 films by reactive magnetron sputtering in a N_2 (40 vol.%)/Ar gas mixture followed by annealing in N_2. They also synthesized N-doped powders by treating anatase TiO_2 in ammonia (67 vol.%)/argon atmosphere at 600 °C for 3 h, respectively. The products contained total N-contents of *ca*. 1 at.%.

* Corresponding author.
E-mail address: j.a.darr@ucl.ac.uk (J.A. Darr).

0955-2219/$ – see front matter © 2009 Elsevier Ltd. All rights reserved.
doi:10.1016/j.jeurceramsoc.2009.02.008

The same group suggested that active sites for photocatalysis in visible light were due to the substitutional nitrogen in the oxide lattice. Since this work, the range of doping concentrations reported recently for active photocatalysts has been very narrow, generally lower than 1 at.%.[13,22–24]

Nitrogen-doped TiO_2 has been reported in the literature as having been made by a range of methods such as plasma nitridation of pure Ti-rod with cathodic arc deposition,[28] annealing TiO_2 or Ti-compounds at elevated temperatures under ammonia gas flow,[23,24] sol–gel processes using N-containing precursors,[29] annealing TiN in air,[30] pulsed laser deposition (PLD) using a TiN target in an oxygen/nitrogen gas mixture,[31] chemical vapour deposition (CVD) using titanium metal-organic precursors in NH_3 gas[32] and ion-beam-assisted deposition (IBAD) of TiO_2 vapour in the presence of nitrogen ions.[22] The particle sizes of the products are reported to range from *ca*. 20 to 200 nm.

Phase-pure titanium nitride (TiN) and TiO_2 with higher than a few at.% N-loadings are also of interest in other applications such as the preparation of conductive materials, anti-wear and anti-corrosion coatings.[33–35] In general, phase-pure TiN tends to be made under more severe conditions than low level N-doped titania, *e.g*. reactions require higher temperatures, involve high-energy processes or are carried out in vacuo (to eliminate reoxidation). The common methods of synthesizing pure titanium nitride (rather than low level N-doped titania) include physical vapour deposition (PVD),[36] reactive sputtering,[37] cathodic arc deposition,[38,39] plasma-gas reaction,[40] and CVD.[41] Methods such as PVD and CVD are less effective in synthesizing nano-sized products (products tend to be in the μm size range).[34,41] TiN powders prepared by plasma-gas phase reaction have a smaller particle size (*ca*. 10 nm) but they also have a high oxygen content (*ca*. 15–20 at.%).[40]

In this work, we report a simple method for the synthesis of N-doped titania and TiN powders from nano-TiO_2 by just varying the gas phase nitridation temperatures. The starting material, crystalline nano-TiO_2, was made as a slurry in a continuous hydrothermal flow synthesis (CHFS) reactor. The crystalline freeze-dried nano-TiO_2 had a large surface area (*ca*. 290 $m^2\ g^{-1}$) and small particle size (*ca*. 4.8 nm by HR-TEM).[42] The nitride materials were prepared *via* heat-treatment of nano-TiO_2 in a tube furnace under a flowing ammonia/argon gas atmosphere at temperatures in the range 100–1100 °C. Using this simple nitridation method, products containing different N-loadings were obtained within 5 h. The photocatalytic activity of N-doped titanias towards decolourisation of a model dye was evaluated under irradiation by visible light.

2. Experimental details

2.1. Chemicals and materials

Titanium (IV) bis(ammonium lactato) dihydroxide (hereafter known as TiBALD, 50 wt.% in water) was obtained from Sigma–Aldrich (Dorset, UK). Mixed ammonia/argon (60/40 vol.%) gas was obtained from BOC (Surrey, UK), with purity quoted at being higher than 99%. Methylene blue (high purity, ≥99.9%) was obtained from Acros Organics (UK). All chemicals were used as received.

2.2. Equipment and techniques

Freeze-drying was performed using a Vitris Advantage Freeze-Dryer, Model 2.0 ES, supplied by BioPharma. The the solids were freeze dried for 22.5 h at 133 Pa after an initial freezing step at −60 °C. Nitridation of TiO_2 was performed in a Lenton tube furnace (Model LTF17/75/600, UK) in an ammonia/argon (60/40 vol.%) gas mixture under flow rates of 200 mL min^{-1} (or in selected cases where stated herein, at 100 mL min^{-1}).

X-ray powder diffraction (XRD) data were collected on a Siemens D5000 X-ray diffractometer using Cu Kα radiation (λ = 0.15418 nm). Data were collected over the 2θ range 20–80° with a step size of 0.02° and a count time of 2 s. Crystallite size was calculated from XRD peak half-widths using the Scherrer equation.[43] Particle size and morphology of selected nanopowders were investigated using a JEOL 2010 transmission electron microscope (200 kV accelerating voltage). Samples were collected in carbon coated copper grids (Holey Carbon Film, 300 mesh Cu, Agar Scientific, UK) after being briefly dispersed ultrasonically (Kerry™ ultrasonic bath, 30 W) in 15 mL ethanol for 3 min. Brunauer–Emmett–Teller (BET) surface area measurements were performed on a Micromeritics Gemini analyser. The powders were degassed at 120 °C in N_2 (BOC, UK) for 12 h prior to BET analyses.

UV–Vis absorption spectra of methylene blue (MB) solutions were recorded using a PerkinElmer (Lambda 950) UV–Vis spectrophotometer. The UV–Vis absorption spectra of the powdered samples were measured using an integrating sphere accessory by the diffuse reflectance method. The CIE Lab colour parameters, *L*a*b**, were calculated from these data using a COLOUR® software (PerkinElmer, UK). The UV–Vis data were recorded in the range 320–800 nm using Spectralon blank as reflecting standard and a D65 standard illuminant with a 10° viewing angle. The chromatic coordinates of the samples were recorded. Additionally, the band-gaps were calculated using the Kubelka–Munk function via conversion of the reflectance spectra into the equivalent absorption coefficient for indirect transition.

Raman spectra of all samples were recorded at room temperature with a Renishaw InVia™ Raman microscope system equipped with a 1200 lines mm^{-1} grating and a diode laser operating at 785 nm. The spectral resolution and precision of the instrument were 1 cm^{-1}. Measurements were carried out on powdered samples at a low laser power of *ca*. 1.0 mW to avoid oxidation of the TiN phase by laser heating.

The X-ray photoelectron spectroscopy (XPS) experiments were performed on a Kratos Axis Ultra-DLD photoelectron spectrometer using monochromatic Al Kα radiation (photon energy 1486.6 eV). Survey scans were performed at a pass energy (PE) of 160 eV, whilst detailed scans were performed at PE 40 eV. All data were analysed using CasaXPS™ software (Version 2.3.13 dev). All data were calibrated to the C(1 s) signal, which was assigned a value of 284.7 eV, and attributable to adventitious carbon. Curve fits were performed using a Shirley

background and a Gaussian peak shape with 30% Lorentzian character.

Energy-dispersive X-ray (EDX) spectroscopy coupled with scanning electron microscopy (SEM) was conducted on a JEOL 5410LV SEM instrument, equipped with an Oxford Instruments Inca 400 EDX unit operating at 25 kV and 15 mm working distance. Samples for SEM were mounted on an aluminium stub and evaporatively coated with carbon. Averages of 10 area scans (1 μm × 1 μm areas) were used to calculate average elemental compositions.

The photocatalytic activity test system consisted of eight 50 mL glass beakers as reactors (Duran™) and a overhead fan-cooled 400 W high-pressure Hg lamp (400HPLR, Philips, RS Components; radiation λ_{max} = 360–720 nm). A 23 cm diameter (0.4 cm thick) round frosted glass screen[a] (First Mirrors, Bow London) was used to act as a light diffuser and ensure even illumination. *Note*: The light diffuser was shown also to remove *ca.* 40% of wavelengths shorter than 400 nm. Despite the use of the diffuser, the Hg lamp emits at several wavelengths in the visible range so the samples are exposed mainly to visible light, with a reduced UV component. It was placed directly above the photocatalytic reactors (2.0 cm from the lamp and *ca.* 1.5 cm above the liquid level). An irradiation intensity of *ca.* 2.7 mW cm^{-2} was measured by a UV meter (UV intensity meter model J-221 Ultraviolet Products, Cambridge UK) when placed under the light diffuser at a distance of 1.5 cm (the liquid level). The photoreactors were placed on a magnetic stirrer (RET C, IKA-WERKE®) and 1.5 cm long magnetic fleas were added to each reactor. The reactors had access to air at all times and a stirrer speed level of 250 rpm was used for the experiment. Under initial tests, the system was validated and shown to give even light distribution and reproducibility in each position of the photoreactor via a photocatalytic test using identical TiO_2 samples and MB solutions.[44]

2.3. Synthesis of nano-TiO_2 using CHFS

The nano-TiO_2 starting material was made using a CHFS system, the basic design of which was reported elsewhere (Fig. 1).[45–49] Briefly, the details of the system are as follows; the CHFS system incorporates three Gilson 305 HPLC pumps fitted with 25 mL pump-heads, 316SS Swagelok™ 1/8 in. fittings and tubing, except the counter-current mixing point (R in Fig. 1) and electrically powered water preheater (H in Fig. 1) which are built from 1/4 in. fittings. For the synthesis of nano-TiO_2, an aqueous solution of TiBALD (0.4 M) was pumped to meet a flow of water at room temperature at a T-junction (Fig. 1) and this mixture was then mixed with a stream of supercritical water at the reaction mixing point (a counter-current mixer[45,50]), whereupon rapid precipitation of crystalline anatase occurred. The nano-TiO_2 suspension was then cooled in flow *via* a water jacket cooler and an off-white slurry was collected at the exit of the back-pressure regulator (after first passing through the in-line Swagelok™ 7 μm filter to remove any larger aggregates). The supercritical water feed was at 400 °C and 24.1 MPa (*Note*: The critical temperature and pressure for water are T_c = 374 °C and P_c = 22.1 MPa),[51–53] whilst the other liquid feeds were at room temperature initially. HPLC pump rates of 20, 10 and 10 mL min^{-1} were used for supercritical water (*via* pump 1), titania precursor (TiBALD) solution (pump 2) and the cold water feed (pump 3), respectively. The third feed (pump 3) was used in order to give in-line dilution and so that direct comparisons could be made to other work.[42] Slurries were then centrifuged (5100 rpm for 60 min), washed twice and freeze dried at *ca.* 133 Pa overnight (22 h). According to the mass of the dry powder, the yield was calculated as *ca.* 90%.

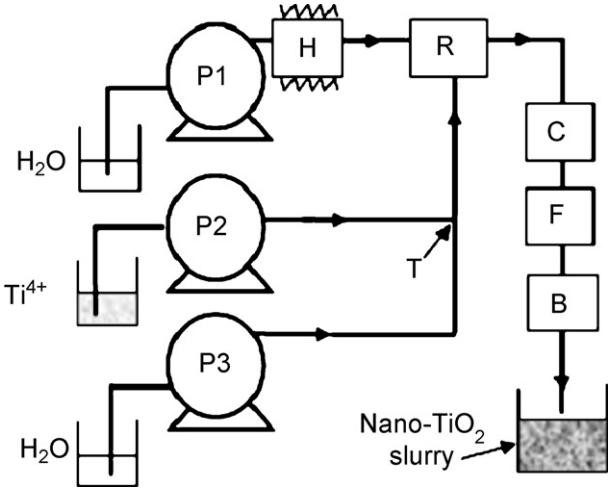

Fig. 1. Schematic representation of the three-pump (P1, P2 and P3) continuous hydrothermal flow synthesis system that was used to prepare nano-TiO_2. Key: P = pump, C = cooling, F = filter, B = back-pressure regulator, T = T-junction, R = reactor, H = heater.

2.4. Synthesis of N-doped TiO_2 and TiN powders

Freeze-dried nano-TiO_2 powder (*ca.* 0.5 g), synthesized by CHFS, was placed on a platinum plate before being transferred into the tube furnace (Model LTF17/75/600, UK). Initially, a flow of ammonia/argon (60/40 vol.%), at a rate of 50 mL min^{-1} was maintained for 60 min through the tube to remove air and water. After a brief period for stabilization of the gas flow to 200 mL min^{-1}, the furnace was heated from room temperature to a set point at the rate of 10 °C min^{-1} (the set-points ranged from 400 to 1100 °C over all the experiments). The data herein are largely for the samples up to 1000 °C with selected information on the 1100 °C sample also being given. The set-point temperature was maintained for up to 5 h, whereupon the furnace was allowed to cool at 20 °C min^{-1} under the same gas flow. The photocatalysts obtained were ground with an agate mortar before use.

2.5. Photocatalytic decolourisation of methylene blue

The powdered catalysts were screened for photocatalytic activity by measuring the decolourisation of methylene blue

[a] Experiment was undertaken in the dark for the first 30 min, and then irradiated in the light.

(MB) in the presence of an illuminated catalyst.[42] 38.6 mg of MB hydrate powder was accurately weighed and added to 2000 mL of deionised water, to give a 6.01×10^{-5} M standard solution. A calibration curve for MB solutions was established by dilution of the MB standard and measurement of the corresponding absorbance at 665 nm (correlation coefficient of 0.998). A 50 mL aliquot of standard MB solution was added into each glass beaker along with 10 mg of the particular powdered sample. The mixtures were stirred (magnetic stirrer) for 30 min in the dark to allow adsorption–desorption equilibrium of dye on the catalyst surface to be established (this was also studied in the following section). After this time, a 5.0 mL aliquot was taken from each reactor and centrifuged (5100 rpm for 5 min) to allow the catalyst to settle. The clear supernatant from this sample was analysed using a UV–Vis spectrophotometer, with the measured intensity of the absorbance band at 665 nm being used to calculate the concentration of MB in the sample. All solids and liquids were then returned to the corresponding reactor. The photocatalytic reactors containing the catalyst were irradiated (open to the air) and stirred continuously. At regular 60 min intervals up to 4 h, the light was switched off and the absorbance of the 665 nm UV–Vis band was measured for each centrifuged sample as described above. The calculated photodecolourisation rate for each sample (assuming a first-order reaction) of the MB for 4 h light irradiation are given in Fig. 11. In each case, the standard deviation in the rate constants assuming first-order kinetics was *ca.* $\pm 1.0 \times 10^{-6}$ s^{-1} and the % (standard) error is *ca.* 13.6% for all samples plus MB.

3. Results and discussion

The nano-TiO_2 made in the CHFS system was obtained as an off-white powder in high yield (*ca.* 90%) and represents a novel material to use for N-doping due to it being crystalline phase-pure anatase with a very high BET surface area (*ca.* 290 m^2 g^{-1}). Identical nano-TiO_2 samples were heat-treated in an ammonia/argon gas flow under different conditions (varying temperature, time and gas flow). The colours of powders ranged from off-white for the precursor nano-TiO_2, to black or dark brown for pure TiN that had been obtained by nitridation at 900 and 1000 °C, respectively (5 h at a gas flow rate of 200 mL min^{-1}). This gas–solid synthesis method was first developed by Ramanathan and Oyama[24] who obtained particles of TiN (particle size: 41 nm; surface area: 28 m^2 g^{-1}) from a starting material of TiO_2 under a flow of ammonia (99.99% purity) gas at 950 °C/10.1 MPa for 1.5 h. In the same report, it was suggested that the nitride particles exhibited low agglomeration and a narrow particle size distribution.[54] Chen et al.[55] used an analogous method to synthesise nitride powders by nitridation of nano-TiO_2 under a gas flow of pure ammonia. The reaction transformed anatase to cubic TiN when the temperature was higher than 770 °C.

In this work, UV–Vis spectra measured by diffuse reflectance of the heat-treated samples and nano-TiO_2 are presented in Fig. 2. The absorbances were determined and the band-gap edge positions were calculated.[56,57] Samples nitrided at 400, 500, 600, and 700 °C showed the band-gap absorption (λ) onset (calculated from the absorption edge and as given in brackets using the Kubelka–Munk model[58] for the samples using the reflectance spectrum) were at 420 (394), 451(403), 485(407), and 526 (460) nm, corresponding to energy band-gaps of 2.97 (3.15), 2.75 (3.08), 2.56 (3.05) and 2.36 (2.70) eV, respectively. Consequently, the optical absorption edges of these N-doped samples shift to lower energy than that of the precursor nano-TiO_2 [$E_g = 3.25$ eV, $\lambda = 383$ nm (382 nm using the Kubelka–Munk model)], and the absorptions after N-doping are stronger in the visible range. It is expected that heating TiO_2 in ammonia contributes to the red shift because of the narrowing of the band-gap.

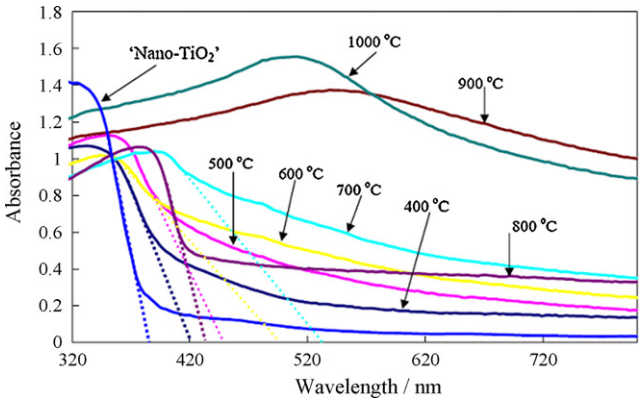

Fig. 2. UV–Vis diffuse reflectance spectra of nano-TiO_2 samples nitrided at different temperatures for 5 h in the range 400–1000 °C, under an ammonia/argon gas mixture for a flow rate of 200 mL min^{-1}.

In the case of the powder nitrided at a temperature of 800 °C (as will be seen later, this is the sample for which most of the anatase to rutile phase transition took place), the absorption edge in the visible range is at 430 nm (2.89 eV), or 413 nm using the Kubelka–Munk model. The samples nitrided at 900 and 1000 °C revealed broad absorption bands across the spectral range due to their dark colour. The colourimetric data for nitrided samples are summarized in Table 1. L^* is the lightness axis (black = 0 to white = 100), a^* is the green (−) to red (+) axis, and b^* is the blue (−) to yellow (+) axis. The N-doped TiO_2 samples which were prepared at 700 °C or below reflected the light essentially in the yellow, ranging from yellowish white (400 °C) to orange brown (700 °C). Upon nitridation in ammonia/argon gas

Table 1
CIE Lab colourimetric parameters of nano-TiO_2 samples which had been nitrided at temperatures in the range 400–1000 °C (5 h in an ammonia/argon gas mixture with a flow rate of 200 mL min^{-1}).

Sample	L^*	a^*	b^*	Colour description
Nano-TiO_2	86.81	−0.87	2.1	Off white
400 °C	85.21	−0.5	7.59	Yellowish white
500 °C	84.49	1.56	7.76	Yellow
600 °C	81.67	2.37	6.88	Dark yellow
700 °C	80	2.21	7.06	Orange brown
800 °C	84.09	−0.55	2.44	Grey
900 °C	67.84	0.16	−1.68	Black
1000 °C	71.39	1.32	−0.63	Dark brown

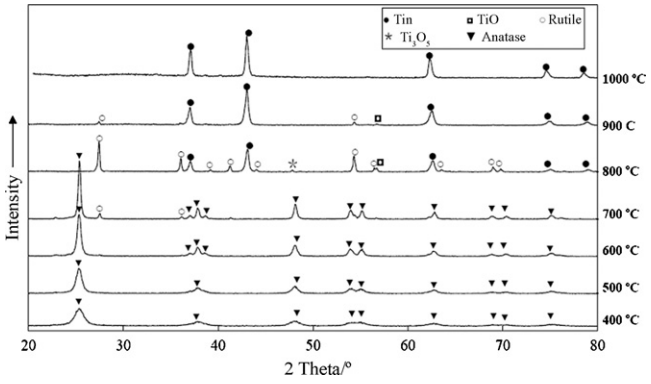

Fig. 3. Room temperature XRD patterns of nano-TiO_2 powders that had been nitrided for 5 h at different temperatures in the range 400–1000 °C in ammonia/argon gas at a flow rate of 200 mL min^{-1}.

from 800 to 1100 °C, the colour went from light grey to dark brown.

The XRD data for nitrided samples (Fig. 3) indicate that single anatase-like phases are present on all samples nitrided at 600 °C and below. Rutile peaks were first observed for the sample nitrided at 700 °C, which was similar to a report by the authors for heat-treatment of nano-TiO_2 powders in air.[42] The ammonia did not appear to have any significant influence on the anatase to rutile transformation temperature. Distinct peaks assigned to TiN (good match to cubic phase JCPDS pattern [38–1420]) appeared in the XRD plot of the sample heat-treated at 800 °C in ammonia/argon gas. A small amount of rutile (TiO_2) was also observed. Additionally, very weak peaks assigned as Ti_3O_5 and TiO, respectively, were observed (these gave a match with JCPDS patterns [23–606] and [12–0754], respectively. The XRD plot for the sample nitrided at 900 °C revealed that the material was almost phase-pure TiN (extremely weak rutile and TiO peaks were also observed). Phase-pure TiN was obtained for the sample heat-treated to 1000 °C in an ammonia/argon gas flow for 5 h. Hence, a likely reaction sequence is as follows: firstly ammonia is decomposed into nitrogen and hydrogen

$$2NH_3 + \text{heat} \rightarrow N_2 + 3H_2 \quad (1)$$

The reaction proceeds with the reduction of TiO_2 to TiO by hydrogen, overall this is as follows:

$$TiO_2 + H_2 \rightarrow TiO + H_2O \quad (2)$$

This reaction to TiO, however, is not a direct one and may proceed through several successive steps that overlap at high temperature. The reduced oxide (Ti_3O_5), though a minor phase, was also observed in our work at 800 °C/5 h in an ammonia/argon gas flow (Fig. 3).

$$TiO_2 \rightarrow Ti_3O_5 \rightarrow TiO \quad (3)$$

$$TiO + NH_3 \rightarrow TiN + H_2O \quad (4)$$

Fig. 4 shows the XRD patterns of the powder produced at 1000 °C for two different dwell times of 3 and 5 h, respectively. When the dwell time was 3 h, more rutile coexisted with the TiN phase (Fig. 4c). By contrast, the rutile phase could not be detected when the nitridation time was increased to 5 h (Fig. 4a).

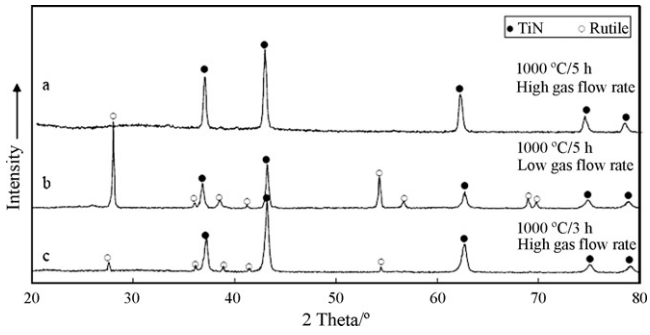

Fig. 4. Room temperature XRD patterns of nano-TiO_2 powders nitrided at 1000 °C in ammonia/argon gas at a flow rate of (a) 200 mL min^{-1} for 5 h, (b) 100 mL min^{-1} for 5 h, and (c) 200 mL min^{-1} for 3 h.

Upon decreasing the ammonia/argon gas flow rate down to 100 mL min^{-1} for 5 h, a significant amount of rutile phase was detected (Fig. 4b).

The above results for XRD were further confirmed by Raman analysis of the products from the nitrided nano-TiO_2 powders (Fig. 5). The Raman spectrum of the precursor nano-TiO_2 anatase powder shows five Raman active bands at ~149 (E_g), 197 (E_g), 396 (B_{1g}), 516 (A_{1g} and B_{1g}) and 641 cm^{-1} (E_g). All samples nitrided at or below 600 °C showed Raman bands due to anatase, which suggests that doped N-atoms are in the lattice. The E_g mode at ~149 cm^{-1} softens (shifts towards lower wavenumbers) as the temperature was increased to 600 °C. The same trend was observed in our previous report on heat-treatment of nano-TiO_2 in air.[42] The softening of this Raman band is attributed to increase in particle size and non-stoichiometry of TiO_2 as it is nitrided in a reducing atmosphere.[59] Upon heating in ammonia/argon gas at or above 700 °C (5 h), the anatase-rutile transition takes place. The Raman spectrum of the sample nitrided at 900 °C revealed peaks due to the TiN phase, along with a weak shoulder at ~447 cm^{-1} due to rutile (E_g band). For the sample nitrided at 1000 °C, three Raman-active bands at ~206, 300 and 569 cm^{-1} were observed and assigned to transverse acoustic (TA), longitudinal acoustic (LA), and transverse optical (TO) modes of TiN, respectively.

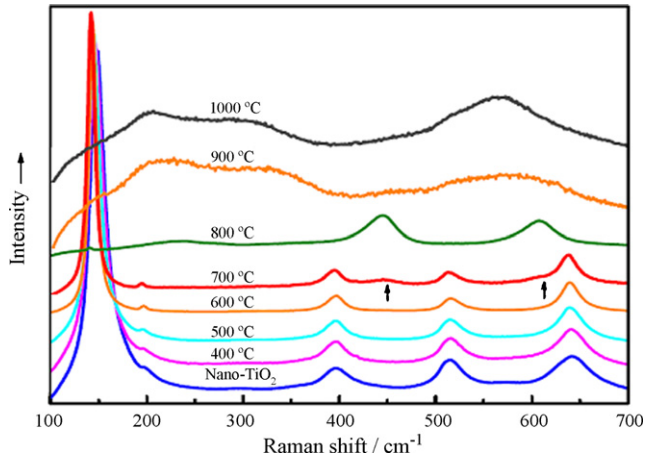

Fig. 5. Room temperature Raman spectra of nano-TiO_2 and samples that were nitrided at different temperatures (400–1000 °C). All samples were heat-treated for 5 h under a gas flow rate of 200 mL min^{-1} in an ammonia/argon gas mixture.

Note that first-order Raman scattering is forbidden for a perfect crystal with a face-centred cubic structure.[60] However, TiN generally contains vacancies and slight N-deficiency which makes defect-induced, first-order Raman scattering in the cubic lattice of TiN possible. We find that the low energy acoustical modes at 225 and 320 cm^{-1} soften as the temperature is increased from 900 to 1000 °C, the softening being attributed to a lesser N-deficiency in the latter.[60]

The crystallite size of N-doped TiO_2 samples was estimated from half-peak widths in the XRD pattern by applying the Scherrer equation[43] and are given in Fig. 6. BET surface area values (N_2 adsorption method) of all nitrided samples generally decreased with increasing temperature and dwell time in the furnace, from 98 $m^2 g^{-1}$ (400 °C, 5 h) to 9 $m^2 g^{-1}$ (1100 °C, 5 h). Fig. 6 shows the relationship between the BET specific surface area, crystallite size (determined from XRD half-peak widths by application of the Scherrer equation), and the nitridation temperature (under the same dwell time of 5 h and ammonia/argon gas flow). Above 900 °C, the crystallite size increased rapidly from 60 nm (at 900 °C) to 108 nm (at 1100 °C).

In this work, pure TiN prepared by heat-treatment in ammonia/argon at 1000 °C for 5 h had an average crystallite size of *ca.* 72 nm and particle size (calculated from the BET surface area assuming a sphere) of 78 nm. The bright-field TEM images (Fig. 7) of the TiN powder (1000 °C for 5 h), revealed polygonal particles with a mean crystallite diameter of *ca.* 72 ± 19 nm (21 particles sampled). Hence, the different methods suggest a similar particle size for the crystallites. In separate experiments, the effects of gas flow rate and nitridation time on crystallite size and surface area were investigated. A nano-TiO_2 powder nitrided at a lower gas flow rate (100 mL min^{-1}) at 900 °C (5 h), had a slightly higher surface area (17 $m^2 g^{-1}$ *versus* 13 $m^2 g^{-1}$) than that made at a higher gas flow rate (200 mL min^{-1}) which reinforces the suggestion by Liu et al.[57] that ammonia gas hinders the coarsening of titania. Such hindrance is expected to lessen (due to the decomposition of NH_3) for longer dwell times and higher temperatures. The hindrance of particle growth can be further confirmed by comparing with previous work of the authors on the heat-treatment of same nano-TiO_2[42] where for samples heat-treated in air (for only 1 h) at 600 and 700 °C, the surface area reduced from 42 to 20 $m^2 g^{-1}$. The same nitridation temperatures (in fact for 5 h) led to a surface area change from 35 to 28 $m^2 g^{-1}$ suggesting that sintering is being effectively hindered for latter sample relative to that heat-treated in air at the same temperature.

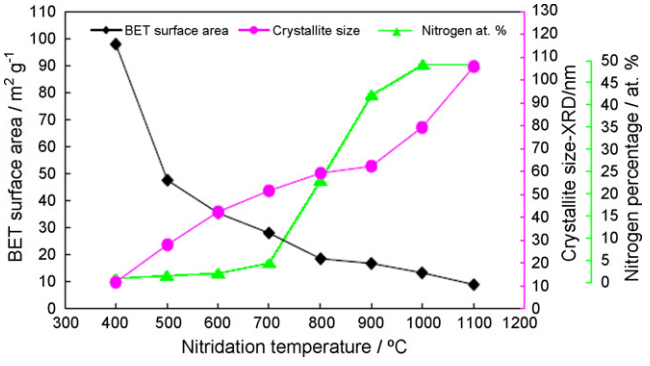

Fig. 6. BET specific surface area, crystallite size (estimated from XRD by Scherrer equation), and nitrogen atomic percentage (quantified by EDX) dependence of nitrided powders prepared at different temperatures. All samples were heated for 5 h under a flow rate of 200 mL min^{-1} of an ammonia/argon gas mixture.

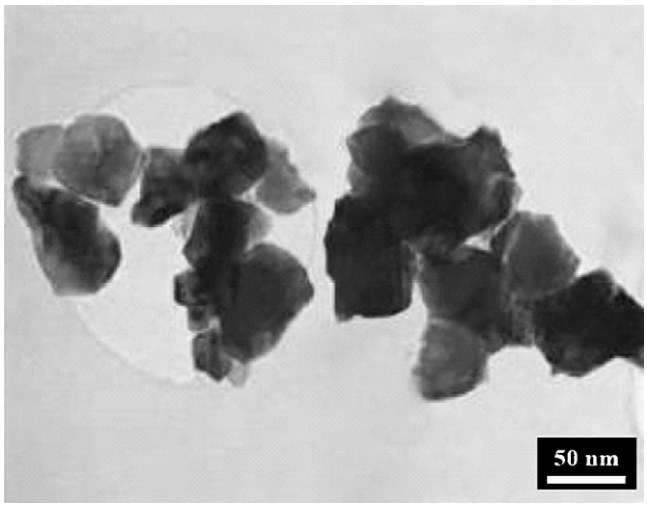

Fig. 7. TEM images of phase-pure TiN prepared in ammonia/argon at 1000 °C, at a gas flow rate of 200 mL min^{-1} mixture over 5 h.

3.1. X-ray photoelectron spectroscopy (XPS)

XPS was applied to examine three main spectral regions of all samples; the Ti 2p region near 460 eV (448–472 eV), the O 1s region near 530 eV (525–539 eV), and the N 1s region near 400 eV (389–418 eV). In these selected regions, the chemical states and quantity of each element on the surface were examined. From the XPS survey spectra of the nitrided samples it can be seen that the surfaces are composed of Ti, O, N and a small amount of adventitious carbon, which was incorporated from the carbon of the starting material.[42]

XPS of the nano-TiO_2 powder was examined in order to assess the amount of Ti^{3+} versus Ti^{4+} ions, as it was assumed that the use of a metal-organic precursor (TiBALD) in the CHFS may provide a slightly reducing environment. The spectrum of the nano-TiO_2 has a Ti $2p_{3/2}$ binding energy of 458.6 eV and a spin-orbit splitting of 5.7 eV between the doublets (Fig. 8a), which is in excellent agreement with the values reported for anatase TiO_2 in the NIST database.[61] This indicates that the material was in a fully oxidised state of Ti^{4+} (O–Ti–O). The same sample also exhibited an O 1s peak at 529.8 eV, characteristic of the oxide. An additional O 1s peak was observed as a higher binding energy shoulder, with a binding energy of 531.0 eV, suggesting the presence of surface hydroxyl groups. The ratio of $Ti:O_{(529.8\,eV)}$ was found to be 1:1.98; thus, the XPS data together with the XRD data, strongly suggest that the nano-TiO_2 material synthesized using the CHFS system is stoichiometric anatase.

Ti 2p spectra from the nano-TiO_2 samples nitrided at different temperatures are shown in Fig. 8. Fig. 8(a) shows the XPS spectra of Ti $2p_{3/2}$ in TiO_2 nitrided at or below 700 °C which can be fitted as one peak located at 458.6 ± 0.2 eV. This peak position

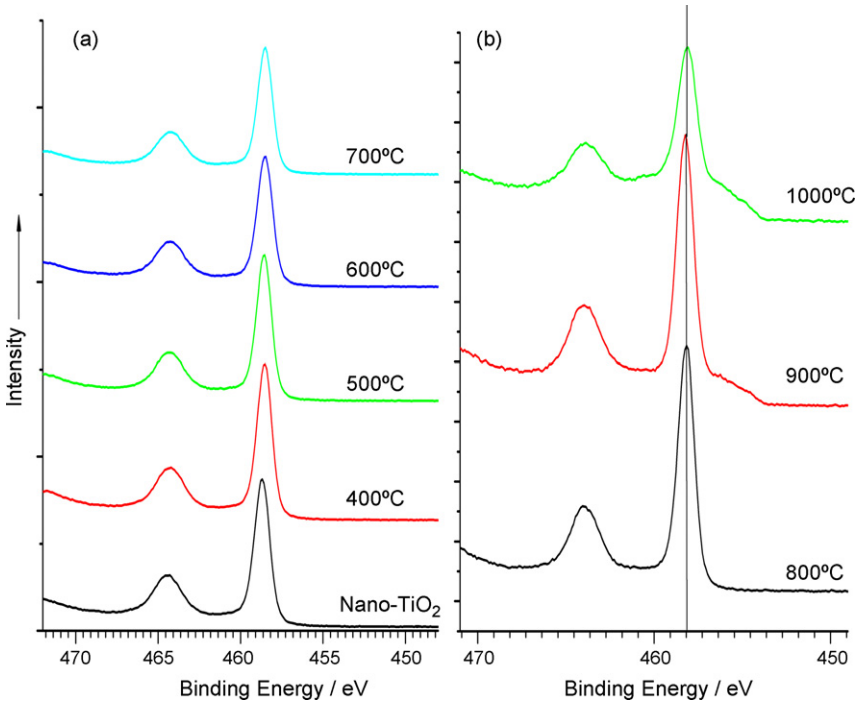

Fig. 8. (a) The Ti 2p peak at 458.6 eV of nano-TiO_2 powder, and powders nitrided at temperatures ranging from 400 to 700 °C. (b) The Ti 2p peak at *ca.* 458 eV for powders nitrided at temperatures of 800, 900 and 1000 °C. All samples were heated for 5 h in an ammonia/argon gas mixture.

is that expected for Ti^{4+} in pure TiO_2 and confirms that no Ti^{3+} is present in the N-doped samples nitrided at temperatures up to 700 °C. Small shifts to lower binding energy (*ca.* 0.4 eV) in the Ti 2p region are noted when comparing the CHFS synthesized nano-TiO_2 to the samples prepared in the range 400–700 °C. The Ti:O ratio (where O is for the oxide component only) remains steady in the range 1:1.96 to 1:1.98 for the samples prepared at temperatures up to and inclusive of 400 °C (by XPS not EDX). For samples prepared at 500 and 600 °C, the ratio is 1:1.92 for both, suggesting that there is some disruption in the lattice arising from the removal of oxygen, hence the lower ratio. For the samples prepared at 700 °C, the Ti:O ratio is noticeably lower at 1:1.68. It is possible that these defect sites are responsible for the photocatalytic activity.[62]

Upon the incorporation of nitrogen into the TiO_2 anatase lattice at nitridation temperatures at or above 800 °C, the Ti 2p spectra exhibit a significant shift from a binding energy of 458.5 (at 700 °C) to 458.0 eV (at 1000 °C), indicating the presence of an ill defined titania phase.[55] For the sample nitrided at 900 °C, a mixture containing TiO_2, TiN and an intermediate phase was obtained; the spectra can be fitted with four doublets [Fig. 10(b)], containing Ti^{4+}, Ti^{3+}, and a titanium species with a lower oxidation state.[55] The fourth doublet, corresponding to the highest binding energy peaks for the Ti $2p_{3/2}$ and $2p_{1/2}$ signals can be attributed to shake-up satellite structure associated with TiN.[62] Upon comparison with the corresponding XRD data, the Ti^{4+} can be correlated to rutile TiO_2, the Ti^{3+} to cubic phase TiN, and the other species could be TiO or some other a distorted lattice Ti species located between the TiO_2 and TiN (*e.g.* titanium oxynitride). For the sample nitrided at 1000 °C, peaks also appeared at a binding energy of 458 eV associated with the Ti^{3+} of TiN, but some Ti^{4+} was also observed, this being attributed to the re-oxidization of the TiN powder surface in air ($G^\circ \sim 580\,kJ\,mol^{-1}$). As XPS is a surface sensitive technique, providing elemental analysis of the upper 5–10 nm layer, this re-oxidation is readily noticeable but of course may not readily be observed in the analogous XRD data.

The N 1s peaks in the XPS are useful in identifying the types of nitrogen present in the samples, *i.e.* in N-doped titania, cubic nitride, or some other N-species.[63] N 1s peaks were observed at a binding energy of 399.7 ± 0.2 eV for samples nitrided at or below 700 °C. Typically such binding energies are characteristic of NH_x and atomic γ–N and such species would be conceivable here due to possible adsorption of residual ammonia. However, closer inspection of the literature indicates interstitial nitrogen, or M–N–O bonds (where M = Si or Ni) in the binding energy range 399.5–399.9 eV. It is conceivable that this binding energy reflects the formation of such bonds here. Surprisingly, there is no obvious peak at 395.9 ± 0.2 eV observed for samples nitrided at or below 700 °C, and assigned to atomic β–N (396 eV) for N-doped samples in most of the literature.[23,64] Instead, a XPS peak at 399.7 eV can be clearly observed, suggesting the presence of chemisorbed atomic γ–N and ammonia species. Fig. 9(a) shows the N 1s XPS spectra of samples nitrided in the range 700–1000 °C. A significant shift in the N 1s peak is observed in this nitridation temperature range, from 399.7 eV (at 700 °C), to 395.5 eV (at 1000 °C). In particular, for samples prepared at 900 and 1000 °C, peaks are centred at 395.7 and 395.5 eV, respectively, which are lower than the literature value for TiN of *ca.* 397 eV.[55,64,65] The shift in the N 1s binding energy is consistent with the multiple states observed in the O 1s spectra. Indeed, for preparation temperatures above 800 °C, there are

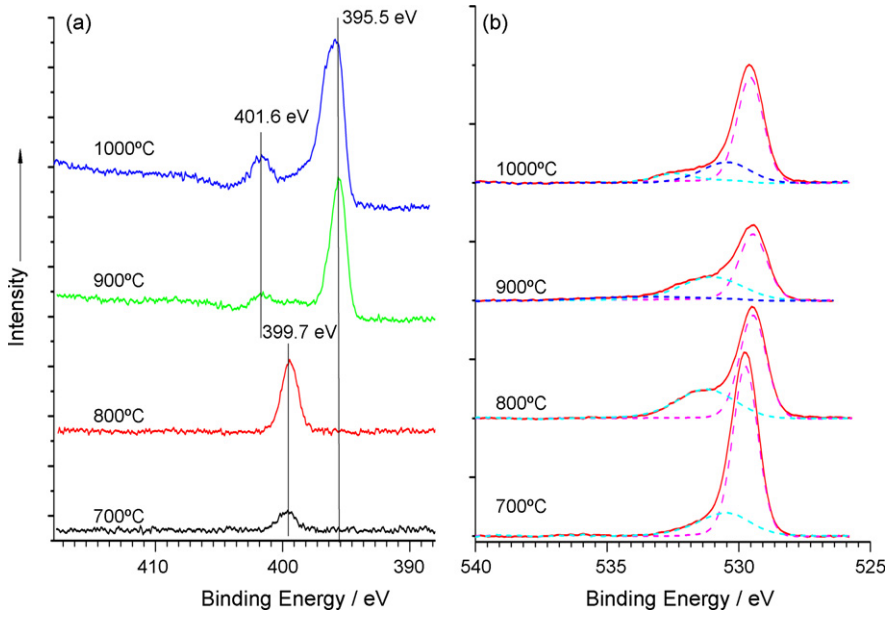

Fig. 9. (a) The N 1s peak of nitrided powders at temperatures ranging from 700 to 1000 °C. (b) O 1s peaks for the same samples. All samples were heated under the gas flow rate of 200 mL min^{-1} in an ammonia/argon gas mixture for 5 h.

2–3 oxygen species present, suggesting oxygen incorporation into the Ti–N lattice.

The O 1s peaks at *ca.* 531–532 eV [Fig. 9(b)] were first observed by Saha and Tomkins[64] and more recently by Gyorgy et al.[66] who assigned them to the formation of oxidized Ti–N, leading to a Ti–O–N structure. The present study suggests that the appearance of this peak is a consistent feature of nitrogen substitution in TiO_2 and signifies the formation of an O–Ti–N structure.[67] This is also supported by the N 1s spectra, whereby the high binding energy peak (401.6 eV), is generally characteristic of N–O bonds (*e.g.* –NOO–), although Saha and Tomkins[64] have suggested that this may be a consequence of terminally bound $–N_2$ adsorbed states.

It is evident also from the N 1s spectra of the sample prepared at 1000 °C, that there are multiple nitrogen states under the main peak at 395.8 eV [Fig. 10(a)]. Curve-fitting analysis reveals two peaks, centred at 395.5 and 396.5 eV; the latter we attribute to a pure nitride as seen in *e.g.* CrN,[68] whilst the former is more perplexing. We believe it to be due to nitride in a non-ideal co-ordination. It has also been proposed by Asahi et al. that N 1s species at ca. 396 eV are assigned to substitutional nitrogen, which may be related to the active sites of the photocatalysis.[23] The other peaks at 397.4 and 399.0 eV, are assigned from the literature, and the energies are analogous to those reported for TiN[69] and BN_xO (here by analogy TiN_xO).[70] Again, the latter oxynitride species would be consistent as a possible intermediate in the re-oxidation sequence to TiO_2. These assignments for the N 1s energies are again in good agreement with the literature for corresponding Ti samples, with Ti $2p_{3/2}$ binding energies of $TiNO_{(x<1)}$ reported to be 454.8 eV and TiN at 455.8 eV.[62] Furthermore, EDX (a non-surface sensitive technique) gave a N/Ti atom ratio of 0.968 (theoretical value = 1) for the sample nitrided at 1000 °C/5 h). Nitrogen at.% quantified by EDX for all nitrided TiO_2 sample are shown in Fig. 6 and samples heat-treated at 400, 500, 600, 700, 800, 900, 1000 and 1100 °C were found to contain 0.92, 1.67, 1.98, 4.36, 22.89, 42.20, 49.07 and 49.11 nitrogen at.%, respectively.

3.2. Photocatalytic decolourisation of methylene blue

Photocatalytic activity of the N-doped TiO_2 and nitrides was assessed on the basis of the decomposition rate of methylene blue (MB) dye under light irradiation for up to 4 h. In order to determine whether the model dye was resistant to degradation under direct light irradiation, an additional 4 h experiment was performed in the absence of any photocatalyst (as a control). It was found that *ca.* 25% of MB was lost due to self-photosensitization as reported previously.[42] Furthermore, it has been also reported that use of methylene blue can lead to erroneous conclusions if oxygen is excluded.[71] Despite this, MB is useful to allow direct comparisons between the different photocatalysts reported herein. All the photocatalytic reactions were undertaken in air, as the photobleaching of MB is irreversible in an oxygen-saturated aqueous solution such as ours.[70]

The photocatalytic reactors containing catalysts were irradiated with visible light after 30 min stirring in the dark to allow the dye adsorption to reach equilibrium onto the catalyst's surface. Thereafter, at 60 min intervals (during irradiation), the light was switched off and the intensity of the 665 nm UV–Vis band absorbance was quickly measured for each sample after first using a short centrifugation step (5100 rpm, 5 min) to remove any solids. All samples were returned after measurement prior to further irradiation. The overall photocatalytic decolourisation rate (during irradiation) of the MB dye for each sample heated at different temperatures was plotted and appeared to obey pseudo-first-order reaction kinetics with a correlation coefficient (R^2) for all the rate constants >0.98.

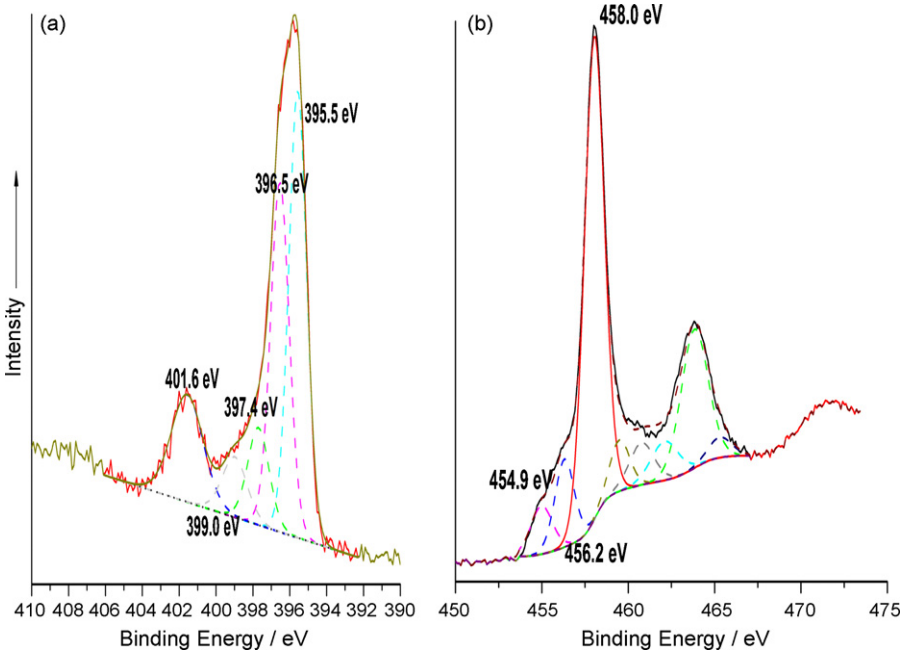

Fig. 10. (a) Curve fitted N 1s spectra for the sample prepared at 1000 °C, and experiencing some re-oxidation. (b) Corresponding Ti 2p spectra showing multiple oxidation states. The samples were heated under a gas flow rate of 200 mL min^{-1} in an ammonia/argon gas mixture for 5 h.

The sample nitrided at 600 °C showed the best photocatalytic activity over the 4 h time-frame of the experiment (Fig. 11), and was higher than that of nano-TiO_2 or its samples heat-treated in air as reported elsewhere by the authors.[42] The material was also partially reduced as a result of the nitridation process. Reduced (non-stoichoimetric) TiO_2 has been shown elsewhere to have a longer lifetime for the holes due to a reduced number of recombination centres.[57] By comparison, the powder treated at 400 °C showed lower photocatalytic activity even though its surface area was higher.

In the case of nitrogen-doped TiO_2, Livrghi et al.[72] proposed that the hole formed by charge separation, results in $N^{\bullet}$ sites (substitutional N at 396 eV in XPS spectra) or N^{-} sites ($N^{\bullet}$ being reduced by the presence of Ti^{3+}). The excited electrons are available for chemical reduction reactions at the surface. In summary, $N^{\bullet}$ centers are formed from visible light absorption with promotion of electrons from the band-gap localized states to the conduction band or to surface-adsorbed electron scavengers ($O_2^{\bullet -}$, $HO_2^{\bullet}$ or $HO^{\bullet -}$ species).[72]

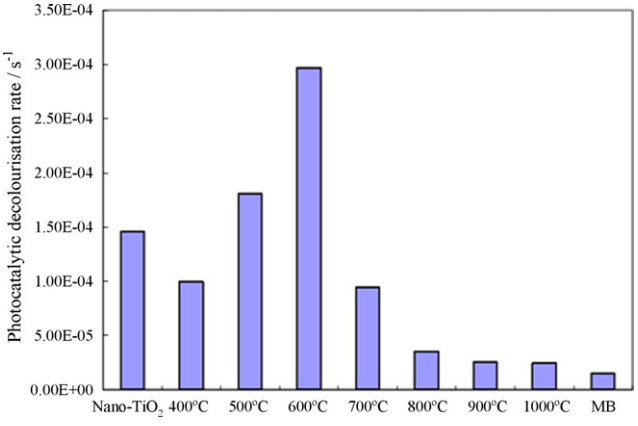

Fig. 11. Photocatalytic degradation rate of the methylene blue dye for nano-TiO_2 and powders nitrided at different temperatures (all at the same gas flow rate of 200 mL min^{-1}, in an ammonia/argon gas mixture with a dwell time of 5 h), as a function of temperature under a visible light source.

The N-doped sample prepared at 600 °C showed significantly higher photocatalytic activity than one prepared at 500 °C, though it possessed larger particle size (46 nm *versus* 31 nm) with similar nitrogen doping levels (1.98 at.% *versus* 1.67 at.%). This can be explained if the predominant mechanism of electron–hole recombination differs depending on the particle size. It is known that within the smaller nanosize catalysts, volume and surface electron–hole recombinations are more likely to take place. Conversely with a slightly larger particle size, the number of active surface sites decreases, and so does its quantum (electron and hole) yield.

A decrease of activity resulting from nitriding the samples at temperatures between 600 and 700 °C, accompanying formation of the rutile phase (Fig. 3), was also observed. This is despite the fact that some of these samples had greater displacement of their absorption edges into the visible range. The TiN samples showed almost no photocatalytic effect.

4. Conclusions

A simple method for the synthesis of nanocrystalline, N-doped TiO_2 and titanium nitride powder was demonstrated. A novel nano-TiO_2 prepared in a continuous hydrothermal flow synthesis system was found to be reactive towards a mixed ammonia/argon flow resulting in N-doping and formation of phase-pure nitride. The route allowed novel N-doped anatase photocatalysts to be prepared with a relatively very small crystallite size (*ca.* 11–52 nm) at 700 °C or less. The sample displaying highest photoactivity (prepared at 600 °C) had *ca.* 1.98 at.%

nitrogen in the titania lattice; this level of N-doping appeared to promote electron transfer from the band-gap localized states to the conduction band or to the surface. Finally, samples prepared at 700 °C appeared to be oxygen deficient, which may be partly responsible for the shifting band-gap and reasonable photocatalytic activity of this sample. Further studies will be required to help clarify whether oxygen deficiency has a bigger effect on photocatalytic activity than N-doping at low levels.

Acknowledgements

EPSRC is thanked for funding the "High Throughput Nanomaterials Discovery" project for developing better photocatalysts [EPSRC Grant Reference: EP/D038499/1] (JAD and JRGE). The Ramsay Memorial Fellowships Trust is thanked for a Fellowship (SB). QMUL is thanked for the College Scholarship (ZZ). Sun Chemicals is also thanked for supporting the industrial case award (JBMG). S. Kellici, M. Phillips, V. Ford, J. Caulfield, M. Willis and Z. Luklinska are thanked for technical assistance. The EPSRC is also thanked by AFC, MB and DJM for the Access to Research Instruments Initiative [EPSRC Grant Reference: EP/F019823/1].

References

1. Pochekovskii, R. A., Lenev, L. M., Antipov, I. V. and Gofman, L. M., Modification of pigment TiO_2. *Inorg. Mater.*, 1977, **13**(4), 548–550.
2. Berenson, M. E., The real value of a TiO_2 pigment. *Plast. Eng.*, 1983, **39**(3), 32–33.
3. Templeton, A., Wang, X. R., Penn, S. J., Webb, S. J., Cohen, L. F. and Alford, N. M., Microwave dielectric loss of titanium oxide. *J. Am. Ceram. Soc.*, 2001, **83**(1), 95–100.
4. Shimizu, Y., Hyodo, T. and Egashira, M., Mesoporous semiconducting oxides for gas sensor application. *J. Eur. Ceram. Soc.*, 2004, **24**(6), 1389–1398.
5. Ruiz, A. M., Sakai, G., Cornet, A., Shimanoe, K., Morante, J. R. and Yamazoe, N., Microstructure control of thermally stable TiO_2 obtained by hydrothermal process for gas sensors. *Sens. Actuat. B*, 2004, **103**(1–2), 312–317.
6. Williams, P. C., Use of titanium-dioxide as a catalyst for large-scale Kjeldahl determination of total nitrogen content of cereal grains. *J. Sci. Food Agric.*, 1973, **24**(3), 343–348.
7. Chen, Y. J. and Dionysiou, D. D., Immobilization of transparent NaNO–TiO_2 photocatalytic films on stainless steel for water purification. *Abstract of papers of Am. Chem. Soc.*, 2005, **229**, 922.
8. Kanki, T., Hamasaki, S., Sano, N., Toyoda, A. and Hirano, K., Water purification in a fluidized bed photocatalytic reactor using TiO_2-coated ceramic particles. *Chem. Eng. J.*, 2005, **108**, 155–160.
9. Mills, A., Elliot, N., Parkin, I. P., O'Neill, S. A. and Clark, R. J. H., Novel TiO_2 CVD films for semiconductor photocatalysis. *J. Photochem. Photobiol. A*, 2002, **151**, 171–179.
10. O'Neill, S. A., Parkin, I. P., Clark, R. J. H., Mills, A. and Elliot, N., Atmospheric pressure chemical vapour deposition of titanium dioxide coatings on glass. *J. Mater. Chem.*, 2003, **13**(1), 56–60.
11. O'Neill, S. A., Clark, R. J. H., Parkin, I. P., Elliot, N. and Mills, A., Anatase thin films on glass from the chemical vapor deposition of titanium(IV) chloride and ethyl acetate. *Chem. Mater.*, 2003, **15**(1), 46–50.
12. Ao, C. H. and Lee, S. C., Indoor air purification by photocatalyst TiO_2 immobilized on an activated carbon filter installed in an air cleaner. *Chem. Eng. Sci.*, 2005, **60**(1), 103–109.
13. Li, D., Haneda, H., Hishita, S. and Ohashi, N., Visible-light-driven N–F-codoped TiO_2 photocatalysts. 1. Synthesis by spray pyrolysis and surface characterization. *Chem. Mater.*, 2005, **17**(10), 2588–2595.
14. Li, F. B., Li, X. Z., Ao, C. H., Lee, S. C. and Hou, M. F., Enhanced photocatalytic degradation of VOCs using Ln^{3+}–TiO_2 catalysts for indoor air purification. *Chemosphere*, 2005, **59**(6), 787–800.
15. Mills, A. and Davies, R., The photomineralisation of reactive black-5 sensitized by titanium-dioxide—a study of the initial kinetics of dye photobleaching. *Photocatal. Purif. Treat. Water Air*, 1993, **3**, 595–600.
16. Mills, A., McGrady, M., Wang, J. and Hepburn, J., A rapid method of assessing the photocatalytic activity of thin TiO_2 films using an ink based on the redox dye 2,6-dichloroindophenol. *Inter. J. Photoenergy*, 2008, **1**, 504945.
17. Choi, J. Y., Kim, K. H., Choy, K. C., Oh, K. T. and Kim, K. N. J., Photocatalytic antibacterial effect of TiO_2 film formed on Ti and TiAg exposed to *Lactobacillus acidophilus*. *Biomed. Mater. Res. Part B*, 2007, **80B**, 353–359.
18. Hajkova, P., Patenka, P. S., Horsky, J., Horska, I. and Kolouch, A., Antiviral and antibacterial effect of photocatalytic TiO_2 films. *Tissue Eng.*, 2007, **13**, 908–1908.
19. Zhang, H. J. and Wen, D. Z., The effect of ZrSiN diffusion barrier on the bonding strength of titanium porcelain. *Surf. Coat. Tech.*, 2007, **201**(9–11), 5720–5723.
20. Curdt, W., Brekke, P., Feldman, U., Wilhelm, K., Dwivedi, B. N., Schuhle, U. and Lemaire, P., The SUMER spectral atlas of solar-disk features. *Solar Galactic Compos.*, 2001, **598**, 45–46.
21. Wu, P. G., Ma, C. H. and Shang, J. K., Effects of nitrogen doping on optical properties of TiO_2 thin films. *App. Phys. A*, 2005, **81**(7), 1411–1417.
22. Matsumoto, Y., Yamaguchi, Y. and Sato, E., Photocatalytic oxidation of sulfur on the doped TiO_2 catalysts. *Bull. Chem. Soc. Jpn.*, 1985, **58**(4), 1255–1258.
23. Asahi, R., Morikawa, T., Ohwaki, T., Aoki, K. and Taga, Y., Visible-light photocatalysis in nitrogen-doped titanium oxides. *Science*, 2001, **293**(5528), 269–271.
24. Ramanathan, S. and Oyama, S. T., New catalysts for hydroprocessing—transition-metal carbides and nitrides. *J. Phys. Chem.*, 1995, **99**(44), 16365–16372.
25. Umebayashi, T., Yamaki, T., Tanaka, S. and Asai, K., Visible light-induced degradation of methylene blue on S-doped TiO_2. *Chem. Lett.*, 2003, **32**(4), 330–331.
26. Yu, J. C., Yu, J. G., Ho, W. K., Jiang, Z. T. and Zhang, L. Z., Effects of F-doping on the photocatalytic activity and microstructures of nanocrystalline TiO_2 powders. *Chem. Mater.*, 2002, **14**(9), 3808–3816.
27. Choi, W. Y., Termin, A. and Hoffmann, M. R., The role of metal-ion dopants in quantum-sized TiO_2—correlation between photoreactivity and charge–carrier recombination dynamics. *J. Phys. Chem.*, 1994, **98**(51), 13669–13679.
28. Huang, A. P., Di, Z. F. and Chu, P. K., Improvement of interfacial and microstructure properties of high-k ZrO_2 thin films fabricated by filtered cathodic arc deposition using nitrogen incorporation. *Surf. Coat. Technol.*, 2007, **201**(19–20), 8282–8285.
29. Ihara, T., Miyoshi, M., Iriyama, Y., Matsumoto, O. and Sugihara, S., Visible-light-active titanium oxide photocatalyst realized by an oxygen-deficient structure and by nitrogen doping. *Appl. Catal. B*, 2003, **42**(4), 403–409.
30. Morikawa, T., Asahi, R., Ohwaki, T., Aoki, K. and Taga, Y., Band-gap narrowing of titanium dioxide by nitrogen doping. *Jpn. J. Appl. Phys. Part 2*, 2001, **40**(6A), 561–563.
31. Suda, Y., Kawasaki, H., Ueda, T. and Ohishima, T., Preparation of high quality nitrogen doped TiO_2 thin film as a photocatalyst using a pulsed laser deposition method. *Thin Solid Films*, 2004, **453–454**, 162–166.
32. Pradhan, S. K., Reucroft, P. J., Yang, F. Q. and Dozier, A., Growth of TiO_2 nanorods by metal organic chemical vapor deposition. *J. Cryst. Growth*, 2003, **256**(1–2), 83–88.
33. Kelly, P. J., Vom Braucke, T., Liu, Z., Amell, R. D. and Doyle, E. D., Pulsed DC titanium nitride coatings for improved tribological performance and tool life. *Surf. Coat. Tech.*, 2007, **202**(3–4), 774–780.
34. Macak, J., Pazderova, M., Jiricek, I., Maly, P., Olysar, K., Cvrcek, L. and Vosta, J., Corrosion properties of physically deposited thin coatings (PVD coatings). *Chemicke Listy*, 2007, **101**(9), 713–721.
35. Wakabayashi, H., Saito, Y., Takeuchi, K., Mogami, T. and Kunio, T., A dual-metal gate CMOS technology using nitrogen-concentration-controlled TiN*x* film. *IEEE Trans. Electron Device*, 2001, **48**(10), 2363–2369.

36. Fortuna, S. V., Sharkeev, Y. P., Perry, A. J., Matossian, J. N. and Shulepov, I. A., Microstructural features of wear-resistant titanium nitride coatings deposited by different methods. *Thin Solid Films*, 2000, **377-378**, 512–517.
37. Perry, A. J., Bull, S. J., Dommann, A., Rafaja, D., Wood, B. P. and Michler, M., The surface damage in titanium nitride associated with lateral sputtering by argon cluster ions. *Surf. Coat. Tech.*, 2000, **133-134**, 253–258.
38. Arias, D. F., Arango, Y. C. and Devia, A., Study of TiN and ZrN thin films grown by cathodic arc technique. *Appl. Surf. Sci.*, 2006, **253**(4), 1683–1690.
39. Chang, Y. Y., Yang, S. J. and Wang, D. Y., Characterization of TiCr(C, N)/amorphous carbon coatings synthesized by a cathodic arc deposition process. *Thin Solid Films*, 2007, **515**(11), 4722–4726.
40. Groza, J. R., Curtis, J. D. and Kramer, M., Field-assisted sintering of nanocrystalline titanium nitride. *J. Amer. Ceram. Soc.*, 2000, **83**(5), 1281–1283.
41. Huang, T. T., Tan, K., Lin, M. H. and Zhang, Q. E., CVD reactions of $TiCl_4$ with ammonia: a quantum chemical study. *Chin. J. Chem.*, 2007, **25**(7), 910–912.
42. Zhang, Z., Brown, S., Goodall, J. B. M., Weng, X., Clark, R. J. H., Evans, J. R. G., *et al.*, Direct continuous hydrothermal synthesis of high surface area nano-sized titania. *J. Alloys Compd.* (in press, available online) doi:10.1016/j.jallcom.2008.09.036.
43. McGehee, R. and Renault, J., Use of standard deviation of X-ray-diffraction lines as a measure of broadening in Scherrer equation—curve fitting method. *J. Appl. Cryst.*, 1972, **50**, 365–370.
44. Chaudhry, A. A., Yan, H., Gong K., Inam, F., Viola, G., Reece, M., *et al.*, Continuous hydrothermal synthesis of high aspect ratio nano-hydroxyapatite rods coprecipitated with calcium doped zirconia, *J. Mater Chem.*, 2009 (under review).
45. Boldrin, P., Hebb, A. K., Chaudhry, A. A., Otley, L., Thiebaut, B., Bishop, P. and Darr, J. A., Direct synthesis of nanosized $NiCo_2O_4$ spinel and related compounds via continuous hydrothermal synthesis methods. *Ind. Eng. Chem. Res.*, 2007, **46**(14), 4830–4838.
46. Chaudhry, A. A., Haque, S., Kellici, S., Boldrin, P., Rehman, I., Fazal, A. K. and Darr, J. A., Instant nano-hydroxyapatite: a continuous and rapid hydrothermal synthesis. *Chem. Commun.*, 2006, **21**, 2286–2288.
47. Weng, X., Boldrin, P., Abrahams, I., Skinner, S. J. and Darr, J. A., Direct syntheses of mixed ion and electronic conductors $La_4Ni_3O_{10}$ and $La_3Ni_2O_7$ from nanosized coprecipitates. *Chem. Mater.*, 2007, **19**(18), 4382–4384.
48. Weng, X., Boldrin, P., Abrahams, I., Skinner, S. J., Kellici, S. and Darr, J. A., Direct syntheses of $La_{n+1}Ni_nO_{3n+1}$ phases ($n = 1$, 2, 3 and infinite) from nanosized co-crystallites. *J. Sol. State Chem.*, 2008, **181**(5), 1123–1132.
49. Chaudhry, A. A., Goodall, J., Vickers, M., Cockcroft, J. K., Rehman, I., Knowles, J. K. and Darr, J. A., Synthesis and characterisation of magnesium substituted calcium phosphate bioceramic nanoparticles made via continuous hydrothermal flow synthesis. *J. Mater. Chem.*, 2008, **18**, 5900–5908.
50. Blood, P. J., Denyer, J. P., Azzopardi, B. J., Poliakoff, M. and Lester, E., A versatile flow visualisation technique for quantifying mixing in a binary system: application to continuous supercritical water hydrothermal synthesis (SWHS). *Chem. Eng. Sci.*, 2004, **59**(14), 2853–2861.
51. Darr, J. A. and Poliakoff, M., New directions in inorganic and metal-organic coordination chemistry in supercritical fluids. *Chem. Rev.*, 1999, **99**(2), 495–541.
52. Cabanas, A., Darr, J. A., Lester, E. and Poliakoff, M., A continuous and clean one-step synthesis of nano-particulate $Ce_{1-x}Zr_xO_2$ solid solutions in near-critical water. *Chem. Commun.*, 2000, **11**, 901–902.
53. Cabanas, A., Darr, J. A., Lester, E. and Poliakoff, M., Continuous hydrothermal synthesis of inorganic materials in a near-critical water flow reactor; the one-step synthesis of nano-particulate $Ce_{1-x}Zr_xO_2$ ($x = 0$–1) solid solutions. *J. Mater. Chem.*, 2001, **11**(2), 561–568.
54. Li, J. G., Gao, L., Sun, J., Zhang, Q. H., Guo, J. K. and Yan, D. S., Synthesis of nanocrystalline titanium nitride powders by direct nitridation of titanium oxide. *J. Am. Ceram. Soc.*, 2001, **84**(12), 3045–3047.
55. Chen, H. Y., Nambu, A., Wen, W., Graciani, J., Zhong, Z., Hanson, J. C., Fujita, E. and Rodriguez, J. A., Reaction of NH_3 with titania: N-doping of the oxide and TiN formation. *J. Phys. Chem. C*, 2007, **111**(3), 1366–1372.
56. Gu, D. E., Yang, B. C. and Hu, Y. D., V and N co-doped nanocrystal anatase TiO_2 photocatalysts with enhanced photocatalytic activity under visible light irradiation. *Catal. Commun.*, 2008, **9**(6), 1472–1476.
57. Liu, G., Li, F., Chen, Z., Lu, Gao, Q. and Cheng, H., The role of NH_3 atmosphere in preparing nitrogen-doped TiO_2 by mechanochemical reaction. *J. Sol. State Chem.*, 2006, **179**(1), 331–335.
58. Kubelka, P. and Munk, F., *Zeit. Für Tekn. Physik*, 1931, **12**, 593–601.
59. Li Bassi, A., Cattaneo, D., Russo, V., Bottani, C. E., Barborini, E., Mazza, T., Piseri, P., Milani, P., Ernst, F. O., Wegner, K. and Pratsinis, S. E., Raman spectroscopy characterization of titania nanoparticles produced by flame pyrolysis: the influence of size and stoichiometry. *J. Appl. Phys.*, 2005, **98**(7), 74305.
60. Spengler, W., Kaiser, R., Christensen, A. N. and Mullervogt, G., Raman-scattering, superconductivity, and phonon density of states of stoichiometric and nonstoichiometric TiN. *Phys. Rev. B*, 1978, **17**(3), 1095–1101.
61. NIST database, http://www.nist.gov, 2008.
62. Liu, H., Ma, H. T., Li, X. Z., Li, W. Z., Wu, M. and Bao, X. H., The enhancement of TiO_2 photocatalytic activity by hydrogen thermal treatment. *Chemosphere*, 2003, **50**(1), 39–46.
63. Glaser, A., Surnev, S., Netzer, F. P., Fateh, N., Fontalvo, G. A. and Mitterer, C., The growth of epitaxial VN(1 1 1) nanolayer surfaces. *Surf. Sci.*, 2007, **601**, 4817–4823.
64. Saha, N. C. and Tompkins, H. G., Titanium nitride oxidation chemistry—an X-ray photoelectron-spectroscopy study. *J. Appl. Phys.*, 1992, **72**(7), 3072–3079.
65. Peng, F., Cai, L., Yu, H., Wang, H. and Yang, J., Synthesis and characterization of substitutional and interstitial nitrogen-doped titanium dioxides with visible light photocatalytic activity. *J. Sol. State Chem.*, 2008, **181**, 130–136.
66. Gyorgy, E., del Pino, A. P., Serra, P. and Morenza, J. L., Depth profiling characterisation of the surface layer obtained by pulsed Nd: YAG laser irradiation of titanium in nitrogen. *Surf. Coat. Tech.*, 2003, **173**(2–3), 265–270.
67. Chen, X. B. and Burda, C., Photoelectron spectroscopic investigation of nitrogen-doped titania nanoparticles. *J. Phys. Chem. B*, 2004, **108**(40), 15446–15449.
68. Nishimura, O., Yabe, K. and Iwaki, M., X-ray photoelectron spectroscopy studies of high-dose nitrogen ion implanted-chromium: a possibility of a standard material for chemical state analysis. *J. Elect. Spectr. Relat. Phenom.*, 1989, **49**(3), 335–342.
69. Biwer, B. M. and Bernasek, S. L., Electron spectroscopic study of the iron surface and its interaction with oxygen and nitrogen. *J. Elect. Spectr. Relat. Phenom.*, 1986, **40**(4), 339–351.
70. Guimon, C., Gonbeau, D., Pfisterguillouzo, G., Dugne, O., Guette, A., Naslain, R. and Lahaye, M., XPS study of BN thin-films deposited by CVD on SiC plane substrates. *Surf. Interf. Anal.*, 1990, **16**(1–2), 440–445.
71. Mills, A. and Wang, J., Photobleaching of methylene blue sensitised by TiO_2: an ambiguous system? *J. Photochem. Photobiol. A: Chem.*, 1999, **127**(1–3), 123–134.
72. Livrghi, S., Paganini, M. C., Giamello, E., Selloni, A., Valenti, C. D. and Pacchioni, G., Origin of photoactivity of nitrogen-doped titanium dioxide under visible light. *J. Am. Chem. Soc.*, 2006, **128**, 15666–15671.